applied sciences

MDPI

Article

Use Your Head? Exploring Configuration-Dependent Variation in Key Fob Range

Mohammad Rezapourian [1,2,*], Erelle Fuchs [1], Martin Volk [1,2], Stefan Klebingat [1,2], Hendrik Mattern [3], Eric Einspänner [1,2,†] and Daniel Behme [1,2,†]

[1] Clinic for Neuroradiology, Medical Faculty, Otto-von-Guericke University Magdeburg, 39120 Magdeburg, Germany; erelle.fuchs@ovgu.de (E.F.); martin.volk@med.ovgu.de (M.V.); stefan.klebingat@med.ovgu.de (S.K.); eric.einspaenner@med.ovgu.de (E.E.); daniel.behme@med.ovgu.de (D.B.)
[2] Research Campus STIMULATE, Otto-von-Guericke University Magdeburg, 39106 Magdeburg, Germany
[3] Department of Biomedical Magnetic Resonance, Otto-von-Guericke University Magdeburg, 39106 Magdeburg, Germany; hendrik.mattern@ovgu.de
* Correspondence: mohammad.rezapourian@med.ovgu.de
† These authors contributed equally to this work.

Abstract

Holding a remote keyless entry fob near the head provides a practical opportunity to investigate configuration-dependent changes in operating range. This pilot study examined five head-contact configurations in nine adults using a factory 433.92 MHz fob and its vehicle. Complementary assessments included an anatomically shaped skull phantom and 7 T magnetic resonance imaging (MRI). Operating thresholds were determined using a staircase procedure. The submental configuration yielded positive gains in all nine participants and the largest mean and median gains: 11.11 m and 12 m, respectively. The within-subject analysis identified an overall difference among configurations in eight complete cases (Friedman $\chi^2(4) = 23.24$; Monte Carlo $p < 0.00001$ based on 200,000 permutations; Kendall's $W = 0.73$). In the phantom series, each condition with distilled water yielded a higher gain than the condition with air at the same location, although gains did not increase consistently across fill levels. These observations identify promising configurations for further investigation. MRI characterized anatomical variation to inform future studies, with no significant associations after correction for multiple comparisons. Each condition was assessed once, and placement was evaluated with fob orientation and hand/body geometry. Building on these observations, repeated measurements with independent control of these factors will help establish repeatability and clarify the electromagnetic contributions.

Keywords: radiofrequency propagation; remote keyless entry; range variation; MRI brain segmentation; skull phantom

Check for updates

Academic Editor: Gerard Ghibaudo

Received: 15 September 2026
Revised: 12 October 2026
Accepted: 20 October 2026
Published: 22 October 2026

Copyright: © 2026 by the authors. Licensee MDPI, Basel, Switzerland. This article is an open access article distributed under the terms and conditions of the Creative Commons Attribution (CC BY) license.

1. Introduction

Remote keyless entry (RKE) systems use low-power radio frequency (RF) transmission to communicate with a vehicle [1]. Communication range depends on the transmitter, receiving antenna, surrounding environment, and their relative geometry [2]. A familiar informal observation is that holding the fob against the head can change the distance at which the vehicle responds. The present study examines this observation through defined contact configurations and an operational range criterion, providing pilot measurements for a phenomenon that has received little direct experimental attention.

Biological tissues are lossy dielectric materials whose electrical properties vary with tissue type and frequency [3–5]. Material near a compact antenna can alter impedance, resonance, efficiency, and radiation pattern [2,6]. These effects do not predict a uniform increase in range: loading, mismatch, absorption, polarization, and shadowing can contribute differently as the overall configuration changes.

Automotive RKE studies offer relevant context. Das and Elfrgani [7] modeled systems at 315 and 434 MHz and showed that human presence and receiver placement can alter predicted coverage. Chen et al. [8] incorporated a key fob, an articulated human model, and a vehicle into a framework for range simulation. Direct measurements of a compact 433 MHz antenna by Buckley et al. [9] demonstrated changes in impedance with body location, separation, and orientation. These studies motivate examining the combined arrangement of the fob, person, and vehicle when interpreting practical range measurements.

Recent work extends this broader context. Experiments with wearable antennas examine body separation and deformation alongside radiation characteristics [10,11], while human body communication experiments demonstrate differences in antenna input impedance between users [12]. Studies of on-body and off-body communication likewise investigate propagation around the head [13]. These systems use different antenna architectures or frequency bands and provide methodological context rather than direct evidence for a 433.92 MHz RKE mechanism. Calibrated tissue-mimicking phantoms offer a complementary route to examining material effects through measured dielectric properties [14–16].

We included an anatomically shaped skull phantom to compare air with distilled water while retaining the external skull geometry. This comparison explores whether the internal medium is associated with a different operating threshold; it is not a calibrated simulation of brain tissue or cerebrospinal fluid (CSF). We also acquired magnetic resonance imaging (MRI) data at 7 T from each participant to characterize anatomical variation. SynthSeg [17,18] and SimNIBS charm [19,20] provide complementary regional and whole-head segmentations. Recent population head modeling work further illustrates the value of documenting anatomical variation and segmentation quality [21], without establishing an RF mechanism from anatomy alone.

The primary question is whether the recorded range gains differ across the tested configurations. The phantom supplies a descriptive internal medium comparison, and MRI provides exploratory anatomical context for future studies. This hierarchy keeps the practical range observations central while distinguishing them from proposed physical explanations.

Summary

- Recorded range gains differed across the tested fob, head, and body configurations.
- The tested submental configuration yielded positive gains in all nine participants and the largest observed mean and median gain.
- At every phantom contact location, each measurement with distilled water yielded a higher gain than the corresponding measurement with air.

2. Materials and Methods

2.1. Human Range Measurements

Nine adults contributed human RKE measurements at a single outdoor site using a VW Touran and its factory 433.92 MHz fob. Five participants were assessed on the first acquisition day and four on the second; participants were not reassessed across days. The vehicle remained in the same location and orientation for all participants.

The five configurations were frontal contact approximately 3 cm above the nasion, right and left temporal contact immediately anterior to the external auditory canal, occipital

contact above the external occipital protuberance, and submental contact immediately dorsal to the jaw. The fob casing was held horizontally in the frontal, temporal, and occipital configurations and vertically in the submental configuration (Figure 1). Casing orientation does not by itself identify the internal antenna's polarization. The participant's orientation relative to the vehicle was maintained during the two temporal measurements. Across all configurations, contact location, casing orientation, and hand/body geometry were not independently manipulated.

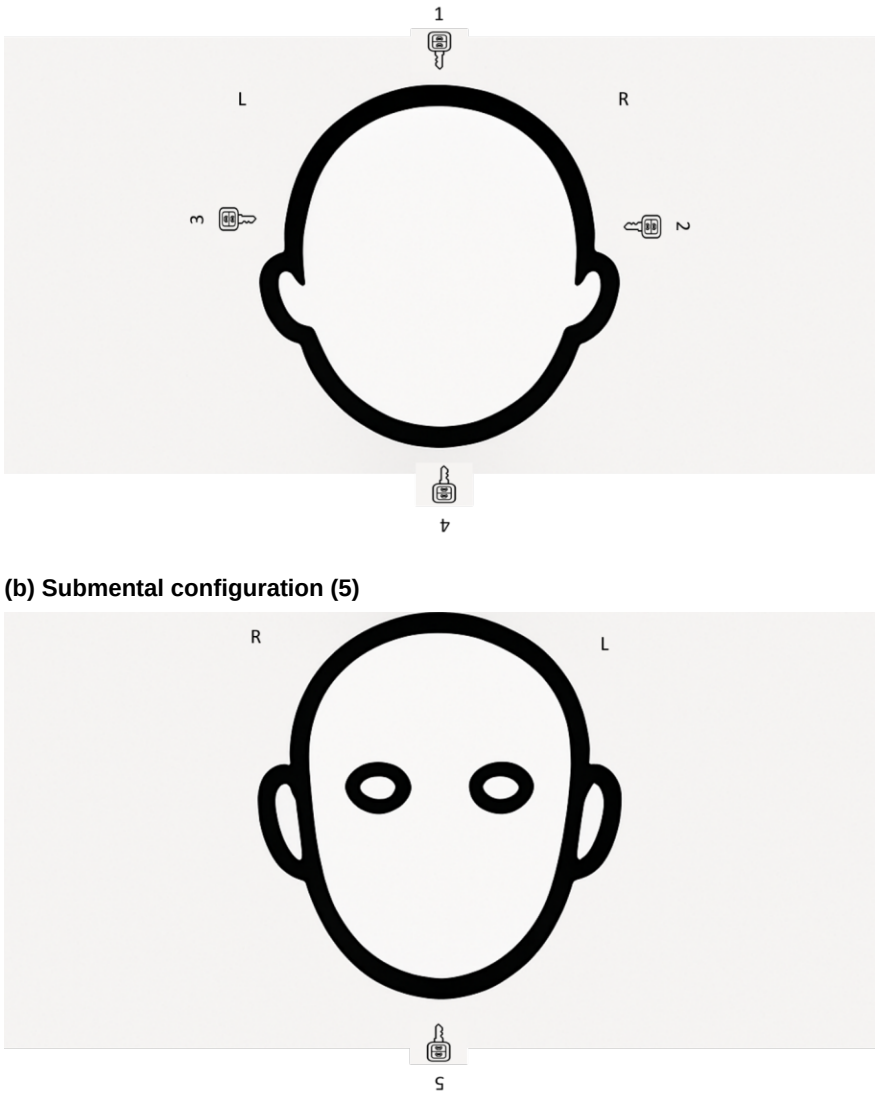


Figure 1. Schematic of the five tested head-contact configurations: 1, frontal; 2, right temporal; 3, left temporal; 4, occipital; and 5, submental. R and L indicate anatomical right and left. Key symbols illustrate contact locations.

The operating threshold was determined by a staircase procedure. Starting near the stationary vehicle, the operator moved away in 5 m increments and tested whether the fob activated the vehicle. When the vehicle no longer responded, the operator moved back toward the vehicle in 1 m increments. The human measurement sheet defines the threshold as the greatest tested distance at which all three activation attempts were successful. These attempts formed the success criterion within one staircase, rather than three independent threshold determinations. Each combination of participant and configuration was measured once. The outcome is therefore a staircase-derived operating threshold along the tested

route, rather than a uniquely established maximum over all greater distances. Endpoint records do not allow retrospective assessment of non-monotonic activation responses.

The source records include a shared no-contact reference, labeled Position 0, and pairs of numerical entries interpreted as a matched no-contact reference and a contact threshold. Here, "no-contact reference" denotes the baseline condition and "contact configuration" denotes the five tested arrangements. The matched reference definition was retained:

$$G_{i,p} = R_{i,p}^{\text{contact}} - R_{i,p}^{\text{reference}}. \quad (1)$$

Here, i denotes a participant and p a contact configuration. Matching may reduce sensitivity to changes in reference range within a session, but the timing of the paired measurements and the reference hand position and fob orientation were not documented. The shared no-contact reference was examined as an alternative definition. The original numerical entries and notation are presented in Appendix A; the corresponding range analysis data and script are available from the corresponding author upon request.

The four occipital entries shown in parentheses were included in the primary analysis as recorded measurements. In each case, the contact threshold was identical to the paired reference, resulting in a gain of 0 m without imputation. A separate occipital entry for participant P06 recorded a contact threshold of 60 m against a reference of 132 m. Because the status of this entry could not be verified, it was excluded from the primary analysis, leaving eight participants with complete measurements across all five configurations. The remaining measurements from P06 were retained in the configuration-specific summaries. Sensitivity analyses examined the effects of excluding the four confirmed zero-gain occipital measurements and, separately, retaining every recorded value, including the unverified entry. The original numerical entries and notation are preserved in Appendix A.

2.2. Phantom Experiment

The same five contact locations were assessed on an anatomically shaped skull phantom using the same VW Touran and RKE system. Four internal conditions were recorded: an air-filled condition and three conditions in which distilled water occupied nominally 80%, 85%, or 90% of the internal volume. Each combination of contact location and fill condition was measured once, yielding 20 contact measurements, each with a paired reference. Gain was calculated using Equation (1). The internal capacity and absolute water volumes were not available in the study records; the percentages are reported as recorded fill conditions rather than calibrated material doses.

2.3. MRI Acquisition and Segmentation

All nine participants underwent structural MRI at 7 T using a magnetization-prepared two rapid acquisition gradient echoes (MP2RAGE) sequence [22]. The stored acquisition metadata identify the scanner as a Siemens 7 T system with an 8Tx32Rx head coil; the model was recorded as "Investigational Device 7T Plus". The MP2RAGE acquisition parameters were as follows: a repetition time of 4.8 s, an echo time of 2.01 ms, first and second inversion times of 0.90 s and 2.75 s, respectively, flip angles of 5° and 3°, an isotropic resolution of 0.7 mm, an acquisition matrix of 320 in the phase-encoding direction, and an in-plane parallel reduction factor of 2. The MP2RAGE uniform (UNI) image was used for subsequent segmentation and morphometric analysis.

Brain parcellation and ventricular measures were obtained with SynthSeg [17,18]. Whole-head tissue segmentation was performed using the charm pipeline in SimNIBS version 4.6 [19,20]. These outputs distinguish regional ventricular CSF measures from the whole-head CSF tissue class; the measures are not interchangeable. SimNIBS-derived intracranial volume (ICV) was defined as

$$\mathrm{ICV} = V_{\mathrm{WM}} + V_{\mathrm{GM}} + V_{\mathrm{CSF}}. \quad (2)$$

The blood class was excluded from this operational ICV definition. In a categorical tissue-label map, blood and CSF labels are mutually exclusive at the voxel level. This avoids double counting but does not establish that excluding intracranial blood yields an unbiased estimate of the entire cranial cavity. SimNIBS ICV ranged from 1264.1 to 1833.6 mL and served as the head-size covariate in the exploratory anatomical screen. Segmentations were visually reviewed as a qualitative plausibility check.

The MRI component complemented the range measurements by characterizing anatomical variation across participants. Figure 2 presents representative MP2RAGE images alongside the corresponding SynthSeg and SimNIBS charm outputs. SynthSeg provided regional brain parcellation and ventricular measures, with different colors distinguishing anatomical labels. SimNIBS distinguished the intracranial white matter, grey matter, and CSF compartments used to estimate ICV, shown in the overlays in lavender, turquoise, and olive yellow-green, respectively. Together, these complementary outputs illustrate the anatomical regions and tissue compartments underlying the volume measures examined in the exploratory analysis of range gain.

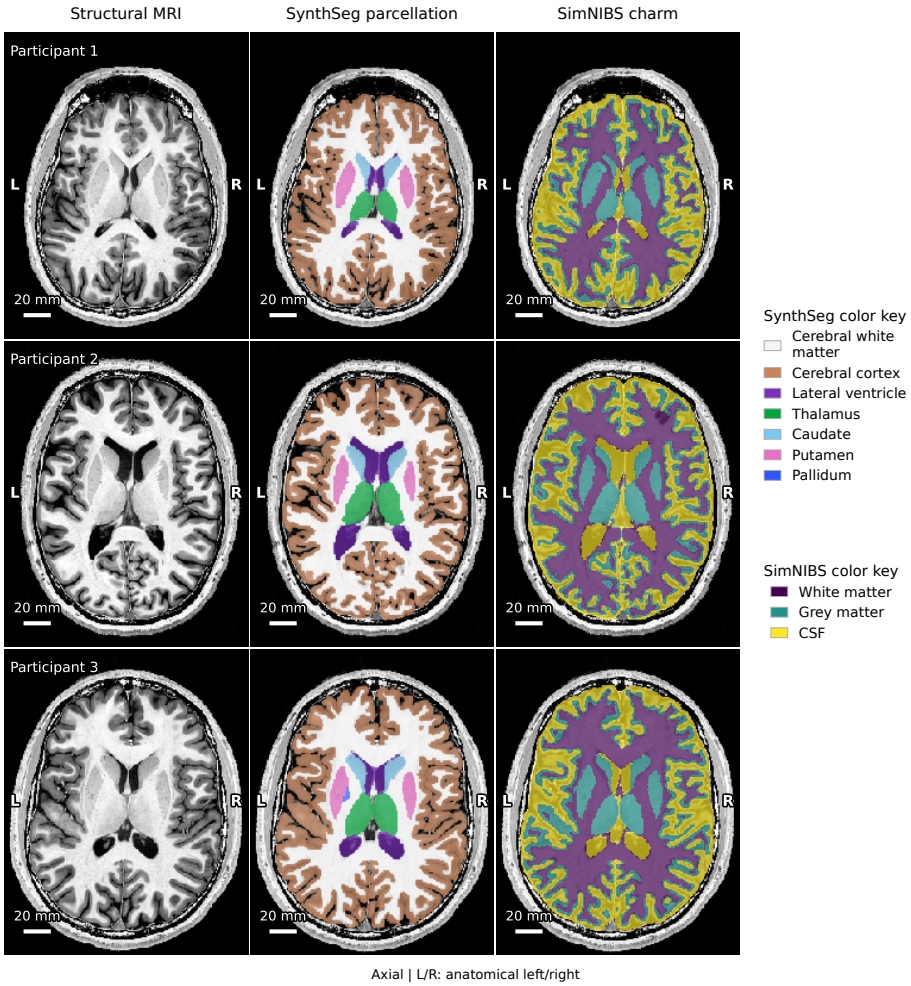


Figure 2. Representative axial 7 T MP2RAGE images and corresponding automated segmentation outputs. Each row presents matching views of the original MP2RAGE image (**left**), SynthSeg brain parcellation (**middle**), and selected intracranial tissue classes from SimNIBS charm (**right**). Each row represents a different participant, with the same axial slice shown across the three columns.

2.4. Statistical Analysis

For each configuration, we reported the number of available observations, mean, median, interquartile range (IQR), minimum and maximum, and counts of positive, zero, and negative gains. The primary omnibus comparison included eight participants with valid measurements in all five configurations. Gains were ranked within each participant using midranks, and the Friedman statistic was corrected for ties. This rank-based comparison does not require equally spaced gain values. The staircase procedure refined thresholds in 1 m steps, producing discrete values and occasional ties. This step size describes the procedural resolution and does not provide an estimate of measurement uncertainty. Means were reported as descriptive averages of the recorded gains.

To calculate a Monte Carlo p-value, we randomly permuted the five configuration labels within each participant 200,000 times. This procedure preserved each participant's observed gains and ties while changing their assignment to configurations. The tie-corrected Friedman statistic was recalculated for every permutation. Under the null hypothesis, configuration labels were assumed to be exchangeable within participants. With b denoting the number of permuted statistics at least as large as the observed statistic and $B = 200{,}000$, the Monte Carlo p-value was calculated as

$$p_{\mathrm{MC}} = \frac{b+1}{B+1}. \tag{3}$$

Permutation p-values were calculated using the plus-one correction to avoid zero estimates [23]. When comparing permuted and observed statistics, a tolerance of 10^{-10} accounted for floating-point rounding. The permutation procedure was implemented in NumPy. The smallest possible estimate was $1/(B+1)$, and Monte Carlo precision depended on the number of sampled permutations.

Kendall's $W = \chi^2/[n(k-1)]$, with $k = 5$, was used to describe concordance in the within-participant configuration rankings. This measure summarizes the observed rankings within the complete-case sample and does not assess measurement repeatability. The Friedman test evaluated overall differences among configurations. Individual configuration rankings, including the submental ranking, were interpreted descriptively because no confirmatory pairwise comparisons were performed.

Four sensitivity analyses examined how data handling and reference choice affected the results: (i) excluding the four confirmed zero-gain occipital entries, leaving four complete cases; (ii) using the shared no-contact reference for the same eight primary complete cases; (iii) using the shared reference after excluding those four measurements; and (iv) including all recorded values, including the unverified 60 m entry. These analyses assessed analytical robustness within the same measurement dataset. The two reference definitions were also compared across 44 paired gains, excluding the unverified entry. We reported a descriptive Spearman coefficient alongside the distribution of paired differences to characterize both correspondence and discrepancies between the definitions. No significance or equivalence tests were applied to these observations, which were clustered within participants.

Acquisition day comparisons were descriptive. For each participant, mean gain was calculated across the available configurations using the primary data definition, which excluded the unverified entry. Because different participants were assessed on the two days, the observed day/cohort contrast could not distinguish acquisition-day effects from differences between participant groups.

In the original exploratory MRI analysis, 10 anatomical measures were examined against seven range outcomes, yielding 70 partial Spearman comparisons adjusted for SimNIBS ICV. The anatomical measures comprised volumes of white matter, grey matter,

CSF, scalp, compact bone, spongy bone, and blood from the whole-head segmentation; total head volume; and ventricular CSF and lateral ventricle volumes derived using SynthSeg. The range outcomes were gains in the five contact configurations, mean gain across all configurations, and mean gain across the two temporal configurations. Benjamini–Hochberg correction [24] was applied across all 70 comparisons.

3. Results

3.1. Configuration-Dependent Range Variation

The primary analysis included eight participants with valid measurements in all five configurations and identified an overall difference in range gain among configurations (Friedman $\chi^2(4) = 23.24$; Monte Carlo $p < 0.00001$). In 200,000 random rearrangements of the configuration labels within participants, none produced a Friedman statistic equal to or greater than the observed value. Applying the plus-one correction gave an estimated p-value of 5.0×10^{-6}, the minimum estimate possible with this number of permutations. Kendall's $W = 0.73$ indicated that the ordering of configurations by gain was broadly similar across participants. These findings describe differences among the recorded configuration-dependent gains and concordance in their within-participant rankings. Because measurement order was not documented and each combination of participant and configuration was assessed only once, the findings do not establish measurement repeatability or isolate a causal effect of anatomical placement.

Figure 3 illustrates the participant-level range gains across the five contact configurations, while Table 1 summarizes all available valid measurements for each configuration. The submental configuration yielded positive gains in all nine participants, with a mean of 11.11 m, a median of 12 m, and an IQR of 8–15 m. Its mean and median were the largest observed configuration summaries. Frontal, right-temporal, and left-temporal mean gains were 6.33, 3.56, and 4.22 m. The eight valid occipital gains had a mean of −1.25 m and a median of 0 m. These are descriptive comparisons with different available-case counts; the omnibus test does not establish every pairwise difference.

Table 1. Human range gain by contact configuration; all distances are in meters. IQR stands for interquartile range.

Configuration	*n*	Mean (m)	Median [IQR] (m)	Range (m)	+/0/−
Frontal	9	6.33	3 [1, 12]	0 to 13	7/2/0
Right temporal	9	3.56	2 [0, 5]	0 to 13	6/3/0
Left temporal	9	4.22	2 [0, 8]	−3 to 15	5/3/1
Occipital	8	−1.25	0 [−2.50, 0]	−7 to 3	1/4/3
Submental	9	11.11	12 [8, 15]	1 to 20	9/0/0

+/0/− denotes counts of positive, zero, and negative gains. IQR endpoints are the 25th and 75th percentiles with linear interpolation; fractional percentiles are summaries, not submeter measurements; n denotes the number of participants contributing one gain observation to that configuration.

Configuration differences were also observed under alternative data and reference definitions. Excluding the four confirmed zero-gain occipital measurements left four complete cases and yielded Friedman $\chi^2(4) = 11.59$, Monte Carlo $p = 0.0059$, and Kendall's $W = 0.72$. Of the 200,000 permutations, 1178 produced a statistic equal to or greater than the observed value. This analysis assessed how omitting those measurements affected the results, although its small sample limited statistical power. Analyses using the shared reference and all recorded values provided further checks of sensitivity to baseline choice and data handling. All these analyses used the same recorded measurements and therefore assessed analytical robustness without providing independent measurement replication.

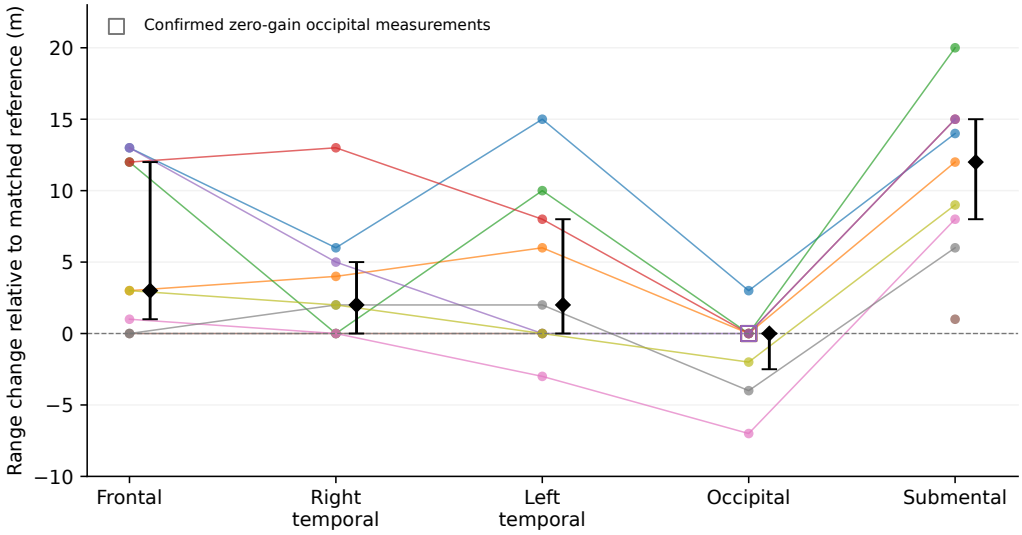


Figure 3. Recorded human range gains across contact configurations. Each colored circle represents a gain calculated from one staircase-derived contact operating threshold and its matched reference. Colors identify participants, and connecting lines link the different configurations measured within each participant. Black diamonds and bars show medians and interquartile ranges (IQRs) of the valid observations.

The two reference definitions gave identical gains for 30 of 44 compared observations. Their descriptive Spearman coefficient was 0.818. The difference between matched-reference and shared-reference gains had a median of 0 m, a mean of 1.66 m, and a range of −1 to 20 m. The largest discrepancy shows that overall similarity does not imply interchangeability of individual gains. Appendix B presents the comparison graph.

Under the primary definition, which excluded the unverified P06 occipital entry, participant mean gains averaged 7.96 m on day 1 and 0.91 m on day 2. The submental configuration had the largest observed mean gain on each day. This difference in absolute gain is a day/cohort contrast: no participant was measured on both days, and the records do not identify its cause.

3.2. Phantom Contrast Between Air and Distilled Water

Figure 4 and Table 2 show the phantom measurements. Gains with the air-filled phantom were negative at all five locations, with a mean of −13.4 m. Among the 15 gains recorded with the phantom filled with distilled water, 12 were positive, 1 was zero, and 2 were negative; the mean gain was 6.5 m. In this single measurement series, every distilled water-filled condition yielded a higher gain than its air-filled counterpart at the same location.

Table 2. Phantom range gain relative to the matched reference (m).

Fill Condition	Frontal	R. Temporal	L. Temporal	Occipital	Submental
Air	−26	−7	−2	−25	−7
80% distilled water	−2	7	13	6	13
85% distilled water	−25	6	14	6	18
90% distilled water	0	9	5	7	20

One gain observation per cell, calculated from one contact operating threshold and its paired reference. Fractions are the nominal recorded fill conditions.

Gain was non-decreasing across the three water fractions at two of five locations. The submental gains were −7 m with air and 13, 18, and 20 m at 80%, 85%, and 90% water. This local progression is descriptive and does not establish a general dose response.

The frontal gain at the 85% fill level remained negative at −25 m, illustrating that the phantom filled with water did not uniformly yield positive gains.

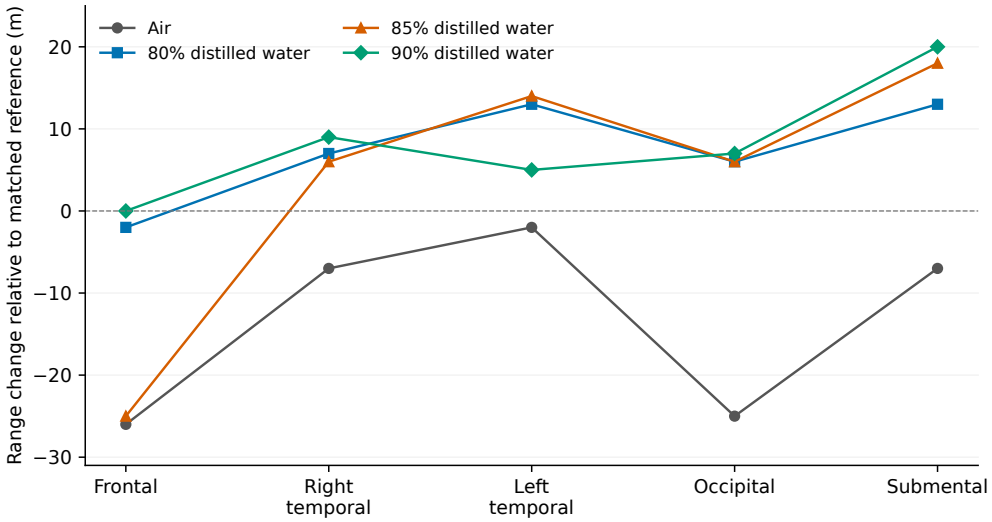


Figure 4. Phantom range gains under the four recorded fill conditions. Each point represents a gain calculated from one staircase-derived contact operating threshold and its matched reference. The vertical axis extends from −31 to 25 m so that the −26 and −25 m observations are fully visible.

3.3. Exploratory Anatomical Characterization

Automated segmentation characterized anatomical variation across the nine participants, with SimNIBS ICV spanning 1264.1–1833.6 mL. In the original MRI analysis, no anatomical association was statistically confirmed after correction across the 70 exploratory comparisons. The MRI component provides descriptive anatomical context and informs hypotheses for prospectively designed studies.

4. Discussion

The main contribution is a set of practical observations showing that the measured operating threshold varies with the tested fob, head, and body configuration. The submental arrangement yielded positive gains in all nine participants and the largest observed mean and median gain. Configuration differences were detectable in the eight complete cases and were also present when confirmed zero-gain entries were excluded and under alternative reference definitions. This provides a concrete basis for follow-up experiments while keeping the descriptive submental ranking distinct from a claim of statistical superiority over every other configuration.

These observations complement electromagnetic and automotive RKE studies that emphasize body proximity and transmitter-receiver geometry [7–9]. The present study adds measurements based on whether the vehicle responded to the fob under practical outdoor conditions. The comparison between reference definitions also demonstrates why future studies should document and standardize the no-contact baseline: reference geometry can shift a configuration-specific gain in either direction, and correlated gain definitions can still disagree materially for individual observations.

The submental arrangement is a promising configuration for further investigation. It combines placement near the lower head and neck with a vertical casing orientation, whereas the other arrangements used a horizontal orientation. The positive human gains and increasing phantom submental gains across the tested fill levels motivate experiments that independently vary orientation and material. The observed advantage belongs to the

combined arrangement; anatomical placement, polarization, and hand/body geometry were not isolated.

Several candidate contributions generate testable predictions. Material loading would predict changes in antenna input impedance or radiated field when the adjacent medium or separation changes while orientation is held fixed [6,9–11]. The phantom contrast is compatible with an internal-medium contribution, but no impedance or field measurement identifies that pathway. An orientation or polarization contribution would predict a change when the fob is rotated at a fixed location with the surrounding geometry unchanged. The vertical submental condition makes this explanation relevant, but the present design does not test it independently. A shadowing or directional-radiation contribution would predict changes with body orientation and transmitter vehicle azimuth [2,7,13]. Low occipital gains are compatible with this possibility, without uniquely demonstrating it. Right and left temporal measurements maintained participant orientation relative to the vehicle, but their similar group summaries do not establish a lateral anatomical advantage. These alternatives need not be mutually exclusive.

The phantom adds a useful descriptive comparison: each gain recorded with distilled water was higher than the gain recorded with air at the same location. Distilled water was an uncalibrated contrast medium, so this result does not identify brain tissue, CSF, or intracranial water as the cause of the human response. The absence of a general gradient across fill levels is also informative, because it directs future work toward the complete geometry and material distribution rather than assuming that more water necessarily means more range. Experiments using tissue-equivalent mixtures with measured dielectric properties [14–16] and a controlled fob orientation would support a more targeted material comparison.

MRI supplies anatomical characterization rather than a confirmed explanation of range variation. Recent segmentation methods and population head models provide tools for future studies of anatomical diversity [17,18,21]. With a small exploratory cohort and many comparisons, prospectively specified endpoints and a larger sample are needed before assessing an anatomical predictor. The anatomical characterization complements the directly observed configuration and phantom contrasts and provides a basis for prospectively specified anatomical hypotheses.

The principal limitations concern measurement repeatability, sample size, and experimental control. With one staircase per condition, within-condition variability and test–retest reliability could not be estimated. Consistency across participants, rank concordance, and sensitivity analyses describe the recorded dataset rather than measurement repeatability. The small cohort also limits precision. Detailed participant demographics and acquisition metadata, including measurement order, weather conditions, posture, handling, separation between the fob and skin, battery condition, and receiver antenna characteristics, were not systematically documented during data collection. Different participants were assessed on the two days, so the observed day/cohort difference may reflect participant variation, handling, battery condition, environmental propagation, or a combination of these factors; neither a pure day effect nor an operator height effect was established. Ground reflection and multipath may produce local fading transitions, meaning that the recorded thresholds characterize performance along the tested route rather than a uniquely established maximum range. Incomplete documentation of the reference geometry also limits interpretation of absolute gains. Finally, the use of one vehicle, fob, site, and phantom geometry constrains generalization. These considerations define the scope of the pilot observations and the priorities for replication.

A focused next study would repeat the threshold measurements using independently initiated staircase procedures, randomize or counterbalance configuration order, document

the baseline and skin separation, and rotate the fob at fixed contact locations. Distance-resolved success rates, additional vehicle systems and sites, calibrated phantoms, and direct impedance, radiated power, polarization, and field measurements could then connect the observed range patterns to their physical contributions. Such measurements would build on the present configuration contrasts while separating measurement variability from mechanism.

5. Conclusions

This pilot study documents configuration-dependent operating thresholds for one factory 433.92 MHz fob and vehicle system at one outdoor site. The tested submental arrangement yielded positive gains in all nine participants and the largest observed mean and median gain. A complementary phantom series showed higher measured gains with distilled water than with air at every tested location, without a consistent gradient across fill levels.

These observations identify specific configurations and material comparisons for controlled follow-up work. They apply to the tested arrangements and do not establish a particular tissue-mediated mechanism or statistically confirmed anatomical predictor. Repeated operating-threshold measurements and independent control of fob orientation, reference geometry, and surrounding material would allow the practical observations to be linked more directly to electromagnetic measurements.

Author Contributions: Conceptualization, E.E. and D.B.; methodology, M.R., E.F., and M.V.; validation, M.R. and D.B.; formal analysis, E.F., S.K., H.M., E.E., and D.B.; investigation, E.F.; resources, E.F., M.V., and E.E.; data curation, E.F., M.V., E.E., and D.B.; writing—original draft, M.R.; visualization, M.R.; supervision, H.M., E.E., and D.B.; project administration, D.B. All authors have read and agreed to the published version of the manuscript.

Funding: This research was funded by the Faculty of Medicine at Otto-von-Guericke University Magdeburg, Germany.

Institutional Review Board Statement: The study was approved by the Ethics Committee of Universitätsklinikum Magdeburg (approval no. 80/25) under the protocol "Korrelation von morphologischen und physiologischen Unterschieden des Gehirns im MRT zur Signalverstärkung eines Funkautoschlüssels" (English translation: "Correlation of morphological and physiological differences of the brain on MRI with signal enhancement of a remote car key").

Informed Consent Statement: Written informed consent was obtained from all participants involved in the study.

Data Availability Statement: The de-identified human and phantom range records, analysis script, and numerical range analysis outputs are available from the corresponding author upon request.

Conflicts of Interest: The authors declare no conflicts of interest.

Abbreviations

CSF, cerebrospinal fluid; ICV, intracranial volume; MRI, magnetic resonance imaging; RKE, remote keyless entry.

Appendix A. De-Identified Source Range Records

Table A1 transcribes the numerical human source entries using newly assigned participant labels. Each paired entry is reported exactly as recorded and is interpreted as reference/contact for the gain calculations.

Table A1. Human source entries (m): shared no-contact reference and paired entries.

Participant	Shared Reference	Frontal	R. Temporal	L. Temporal	Occipital	Submental
P01	140	140/153	138/144	130/145	140/143	140/154
P02	132	132/135	118/122	112/118	118/(118)	119/131
P03	128	128/140	128/128	128/138	127/(127)	127/147
P04	128	128/140	128/141	128/136	128/(128)	127/142
P05	127	127/140	127/132	128/128	128/(128)	127/142
P06	132	132/132	132/132	132/132	132/60	132/133
P07	132	132/133	132/132	133/130	132/125	131/139
P08	132	132/132	132/134	132/134	132/128	132/138
P09	131	131/134	131/133	131/131	132/130	131/140

P01–P05 belong to day 1 and P06–P09 to day 2. The P06 occipital entry is excluded because its status remains unverified.

Appendix B. Comparison of Reference Definitions

Figure A1 compares matched reference and shared reference gains for the observations. Points are clustered within participants and are shown descriptively.

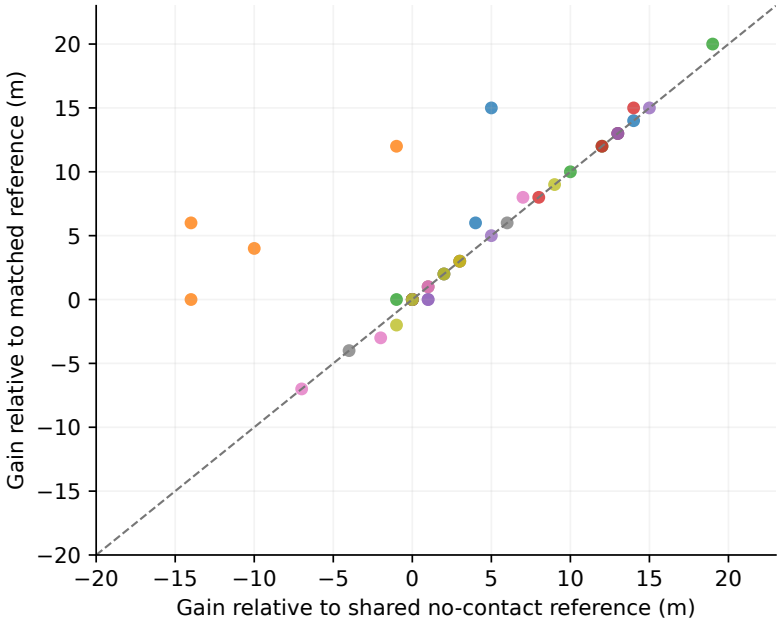


Figure A1. Descriptive comparison of the two reference definitions. Colors distinguish participants. Each point compares gains calculated using the two reference definitions for the same participant and configuration. The diagonal indicates equal gain. Thirty of 44 points lie on the equality line, while individual differences extend to 20 m.

References

1. Garcia, F.D.; Oswald, D.; Kasper, T.; Pavlidès, P. Lock It and Still Lose It—On the (In)Security of Automotive Remote Keyless Entry Systems. In Proceedings of the 25th USENIX Security Symposium, Austin, TX, USA, 10–12 August 2016; pp. 929–944. Available online: https://www.usenix.org/conference/usenixsecurity16/technical-sessions/presentation/garcia (accessed on 8 August 2026).
2. Hall, P.S.; Hao, Y. *Antennas and Propagation for Body-Centric Wireless Communications*, 2nd ed.; Artech House: Norwood, MA, USA, 2012.
3. Gabriel, C.; Gabriel, S.; Corthout, E. The dielectric properties of biological tissues: I. Literature survey. *Phys. Med. Biol.* **1996**, *41*, 2231–2249. [CrossRef] [PubMed]
4. Gabriel, S.; Lau, R.W.; Gabriel, C. The dielectric properties of biological tissues: II. Measurements in the frequency range 10 Hz to 20 GHz. *Phys. Med. Biol.* **1996**, *41*, 2251–2269. [CrossRef] [PubMed]
5. Gabriel, S.; Lau, R.W.; Gabriel, C. The dielectric properties of biological tissues: III. Parametric models for the dielectric spectrum of tissues. *Phys. Med. Biol.* **1996**, *41*, 2271–2293. [CrossRef] [PubMed]

6. Curto, S.; McEvoy, P.; Bao, X.L.; Ammann, M.J. Compact patch antenna for electromagnetic interaction with human tissue at 434 MHz. *IEEE Trans. Antennas Propag.* **2009**, *57*, 2564–2571. [CrossRef]
7. Das, D.; Elfrgani, A. *Antenna Design Methodology for Remote Keyless Entry: The Effects of the Human Body and Vehicular Antenna Positions on Coverage*; SAE Technical Paper; SAE International: Warrendale, PA, USA , 2019. [CrossRef]
8. Chen, S.; Pan, Y.; Sun, H. *CAE Method for Automotive Remote Function Actuator System Range Simulation*; SAE Technical Paper; SAE International: Warrendale, PA, USA, 2022. [CrossRef]
9. Buckley, J.L.; McCarthy, K.G.; Gaetano, D.; Loizou, L.; O'Flynn, B.; O'Mathuna, C. Design of a compact, fully-autonomous 433 MHz tunable antenna for wearable wireless sensor applications. *IET Microw. Antennas Propag.* **2017**, *11*, 548–556. [CrossRef]
10. Jabbar, A.; Zubair, M.; Naveed, M.A.; Mehmood, M.Q.; Massoud, Y. A photopaper-based low-cost, wideband wearable antenna for wireless body area network applications. *IET Microw. Antennas Propag.* **2022**, *16*, 962–970. [CrossRef]
11. Kundu, S.; Fang, X.; Wagih, M. Sustainable, robust wearable antennas using recyclable liquid metal e-fibres. *Adv. Sustain. Syst.* **2026**, *10*, e70657. [CrossRef]
12. Muramatsu, D.; Sasaki, K. Input impedance analysis of wearable antenna and experimental study with real human subjects: Differences between individual users. *Electronics* **2021**, *10*, 1152. [CrossRef]
13. Särestöniemi, M.; Sayrafian, K.; Sonkki, M.; Iinatti, J. A preliminary study of on/off-body propagation channels for brain telemetry using a flexible wearable antenna. In Proceedings of the 17th IEEE International Symposium on Medical Information and Communication Technology (ISMICT), Lincoln, NE, USA, 10–12 May 2023. [CrossRef]
14. Costanzo, S.; Cioffi, V.; Qureshi, A.M.; Borgia, A. Gel-like human mimicking phantoms: Realization procedure, dielectric characterization and experimental validations on microwave wearable body sensors. *Biosensors* **2021**, *11*, 111. [CrossRef] [PubMed]
15. Xu, G.; Zhang, Q.; Liu, H.; Qiu, B.; Yu, X.; Han, J. Characterization and optimization of dielectric phantom composition for frequency-dependent tissue mimicking. *Mater. Today Commun.* **2024**, *41*, 110443. [CrossRef]
16. Firuzalizadeh, M.; Gaffoglio, R.; Giordanengo, G.; Righero, M.; Zucchi, M.; Musacchio Adorisio, G.; Bellone, A.; Vallan, A.; Perrone, G.; Vecchi, G. Joint optimization of antenna system matching and specific absorption rate focusing in microwave hyperthermia cancer treatment. *Cancers* **2025**, *17*, 386. [CrossRef] [PubMed]
17. Billot, B.; Greve, D.N.; Puonti, O.; Thielscher, A.; Van Leemput, K.; Fischl, B.; Dalca, A.V.; Iglesias, J.E.; ADNI. SynthSeg: Segmentation of brain MRI scans of any contrast and resolution without retraining. *Med. Image Anal.* **2023**, *86*, 102789. [CrossRef] [PubMed]
18. Billot, B.; Magdamo, C.; Cheng, Y.; Arnold, S.E.; Das, S.; Iglesias, J.E. Robust machine learning segmentation for large-scale analysis of heterogeneous clinical brain MRI datasets. *Proc. Natl. Acad. Sci. USA* **2023**, *120*, e2216399120. [CrossRef] [PubMed]
19. Puonti, O.; Van Leemput, K.; Saturnino, G.B.; Siebner, H.R.; Madsen, K.H.; Thielscher, A. Accurate and robust whole-head segmentation from magnetic resonance images for individualized head modeling. *NeuroImage* **2020**, *219*, 117044. [CrossRef] [PubMed]
20. Thielscher, A.; Antunes, A.; Saturnino, G.B. Field modeling for transcranial magnetic stimulation: A useful tool to understand the physiological effects of TMS? In Proceedings of the 37th Annual International Conference of the IEEE Engineering in Medicine and Biology Society (EMBC), Milan, Italy, 25–29 August 2015; pp. 222–225. [CrossRef] [PubMed]
21. Berger, T.A.; Wischnewski, M.; Opitz, A.; Alekseichuk, I. Human head models and populational framework for simulating brain stimulations. *Sci. Data* **2025**, *12*, 516. [CrossRef] [PubMed]
22. Marques, J.P.; Kober, T.; Krueger, G.; van der Zwaag, W.; Van de Moortele, P.-F.; Gruetter, R. MP2RAGE, a self bias-field corrected sequence for improved segmentation and T_1-mapping at high field. *NeuroImage* **2010**, *49*, 1271–1281. [CrossRef] [PubMed]
23. Phipson, B.; Smyth, G.K. Permutation p-values should never be zero: Calculating exact p-values when permutations are randomly drawn. *Stat. Appl. Genet. Mol. Biol.* **2010**, *9*, 39. [CrossRef] [PubMed]
24. Benjamini, Y.; Hochberg, Y. Controlling the false discovery rate: A practical and powerful approach to multiple testing. *J. Roy. Stat. Soc. B* **1995**, *57*, 289–300. [CrossRef]

Disclaimer/Publisher's Note: The statements, opinions and data contained in all publications are solely those of the individual author(s) and contributor(s) and not of MDPI and/or the editor(s). MDPI and/or the editor(s) disclaim responsibility for any injury to people or property resulting from any ideas, methods, instructions or products referred to in the content.